A METHOD OF AERIAL STIV WITHOUT REQUIRING OF GROUND CONTROL POINTS

MASAHIRO HASHIBA
Fukuda Hydrologic Center Co. Ltd.

ICHIRO FUJITA
Faculty of Engineering, Kobe University

NORIYUKI NISHIYAMA
Fukuda Hydrologic Center Co. Ltd.

YOKO OHTA
Ministry of Land, Infrastructure, Transport and Tourism Hokkaido Regional Development Bureau

ABSTRACT

By using a UAV (Unmanned Aerial Vehicle), it is possible to measure the river flow by image velocimetry wherever the place away. However, to perform image analysis, it is necessary to install the ground control point (GCP) in the image and to set the accurate coordinates to run a geometric correction. In this study, we extract as pseudo-GCP the point cloud of the 3D terrain model, which was made by Structure from Motion (SfM) using a post-processed kinematic system by UAV. After we calculated the geometric correction by the pseudo-GCP used point cloud, we analyzed the surface velocity distribution by Space-Time Image Velocimetry (STIV) method. We conducted the field observation in the Ishikari river (The river width was 150m). Firstly, we took a picture by drone in a zigzag direction from the left bank to the right bank with a lap rate of 70-85% and created the mesh of 4cm square. It took within a 20minute for transverse distance was 250m and longitudinal distance was 300m. Secondly, we took a slant angle video by a drone hovering about 30 seconds near the riverbank. Comparing the surveying-GCP and pseudo-GCP, the plane position error and the height error was within 0.10 m. Moreover, the flow velocity error due to the surveying-GCP and pseudo-GCP was within 10%, except for low velocity and discharge was within 5%, regardless of the divided sectional method and DIEX method. We succeeded to calculate surface flow velocity with the minimum error by the STIV method using pseudo-GCP which is no requirement of surveying-GCP.

Keywords: *Image velocimetry , Aerial STIV , UAV , GCP , SfM/MVS*

1. INTRODUCTION

The technology of river flow observation due to image velocimetry had been developed as a non-contact observation. The STIV method developed by Fujita et al. (2007) is flexible to image quality and camera angles because the flow direction is set in advance. Therefore, the STIV method is suitable for observation of river flow and used with various types of cameras and observation methods. Besides, by using the unmanned aerial vehicles (UAVs), it was possible to enter in the event of a disaster or inaccessible place, therefore it expands the possibility of observation. Fujita et al. (2016) developed a high-accuracy and efficient image stabilization to apply the space-time image velocimetry (STIV) to airborne images. However, to perform image analysis, it is necessary to install the ground control point (GCP) in the image and set the accurate coordinates to run a geometric correction. Therefore, though it is necessary to make an on-site survey of GCP, it is not easy to make on-site surveying, it takes a lot of work. In recent years, Structure from Motion/Multi-View Stereo Photogrammetry (SfM/MVS) using the high-resolution image by UAV has been developed, and it has been possible to acquire ground terrain information with high accuracy in a short time. In this study, we developed the method of aerial STIV with no requirement of GCP using the pseudo-GCP from the point cloud of the 3D terrain model by SfM/MVS.

2. EXPERIMENTAL FIELD AND DEVICE

The authors conducted the field study in the Ishikari River, located in Hokkaido, JAPAN. The total catchment area of the Ishikari River is 14300 km2. This experimental point “Hashimoto-Cho” is the gauging point located in the middle of the river, whose distance from the sea is 93.9 km. The river width is 150m. This is the low water condition on September 9, 2019. Our device is as follows; UAV: “Inspire2” is manufactured by DJI Co. Ltd., “Klau PPK system” is a post-processing kinematic system compatible with “Inspire2” manufactured by Klau Geomatics Pty Ltd. Two-frequency GNSS operates completely independently of the UAV system. Electronic reference information is imported by post-processing. SfM/MVS software: “Metashape” is by Agisoft LLC and “Trend-point” is by Fukui computer, Inc.

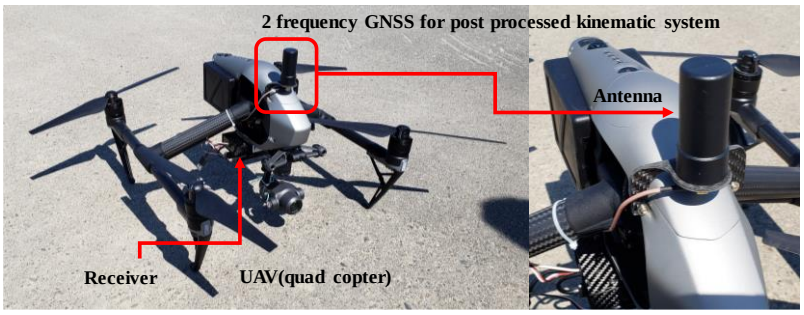

Figure 1. Observation device UAV

3. THE METHOD OF AERIAL STIV

3.1 UAV flight strategy

If it is necessary to cover a river’s width of 200m within the angle of view, the flight altitude is needed 200m above the ground as shown in Figure 2(a). However, as the flight altitude is farther from the ground, the surface waves of the river become invisible. Also, unfortunately, the Japanese aviation law does not allow drone flights over 150 meters above the ground. Therefore, the authors considered two methods. One method is that we operate the UAV to hover at multiple transverse points on the river, we take an image directly below, and then we connect the multiple images as shown in Figure 2(b). Regarding this method, it is needed for the accurate coordinate of the image for connecting multiple images. However, if we take an image that is all of the surface views, it is expected that it will be difficult to work to connect the multiple images without GCP. The second method is that we operate to hover on the riverbank, we take an image from an oblique direction, and then to make an orthoimage using GCP as shown in Figure 2(c). This method requires the creation of an accurate GCP (ground control point) but is simpler than using Figure 2(b) because it uses only one image. We will continue our research in Figure 2(b). However, in this paper, we performed analyses using Figure 2(c).

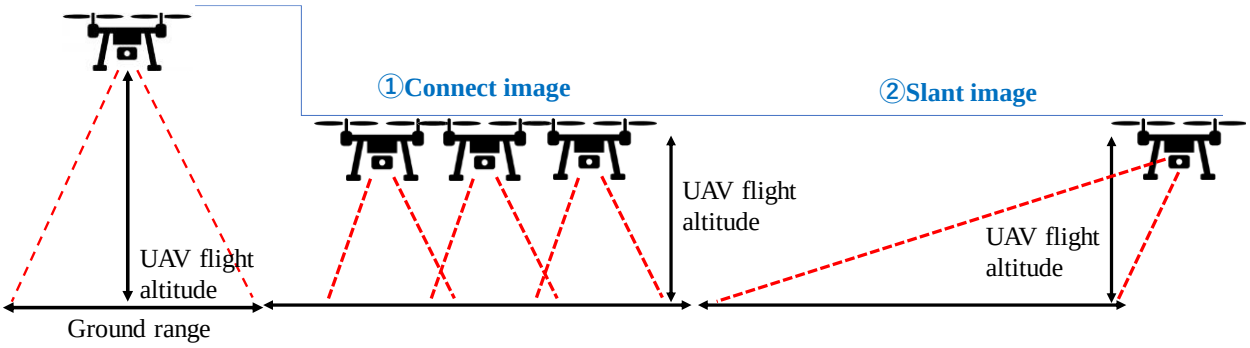

Figure 2. UAV flight strategy

3.2 Method of aerial STIV

The steps for aerial STIV as shown in Figure 3.

1) The UAV flight and hovering on the riverbank will make a video of a slanted image of about 30 seconds. The frame rate is 30 fps and the image resolution is 1920×1080. It is necessary to install GCP on the ground, and it is necessary to measure accurate X, Y, Z coordinates by total station (TS) surveying.

2) Geometrically correct the video based on GCP and set 15 searching lines in the downstream direction. The searching line can be changed arbitrarily depending on the river width.

3) Analyze the brightness change in the STIV method and create a space-time image (STI). In the case of STI, the horizontal axis shows the distance of the searching line, and the vertical axis shows elapsed time. The STI angle (∅) indicates the flow velocity. ∅ was automatically calculated by Fourier analysis obtained from the spectral peaks of the radial component.

$$U = \frac{S_x}{S_t} \tan \emptyset \tag{1}$$

Where U [m/s] is velocity, S_x [m/pixel] is the unit length scale of the line segment, S_t [s/pixel] is unit scale of time axis, $\emptyset$ is angle of STI.

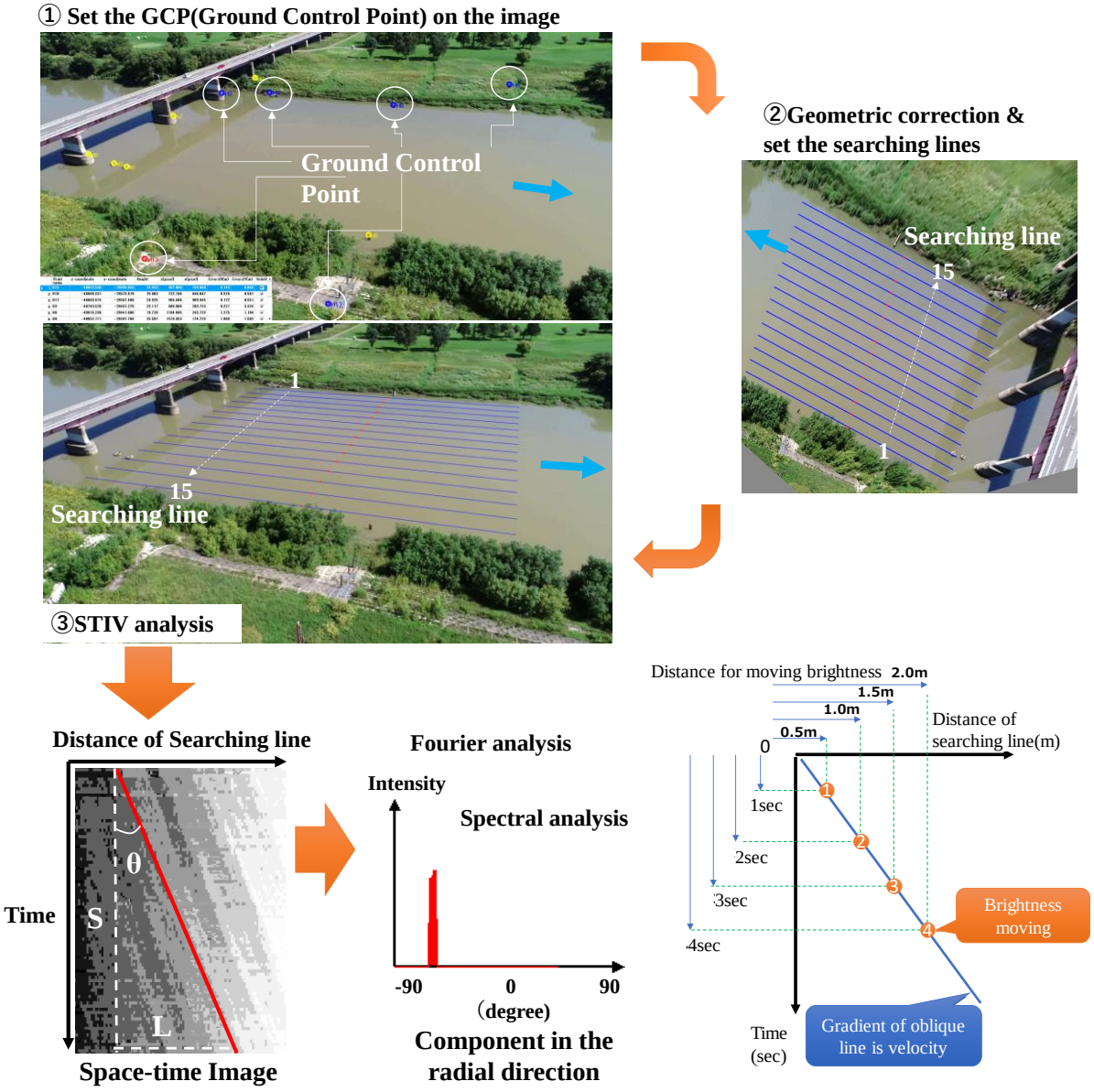

Figure 3. Method of aerial STIV

3.3 Comparison of velocity in distribution multi-angle image

As a first, we verified the surface velocity distribution and discharge obtained by aerial STIV in case of changing the altitude of UAV. The image video was acquired at 5 altitudes (20～130 m above the ground) of the slant view and the ortho view at 2 altitudes (100～130 m above the ground) as shown in Figure 4. Figure 5 shows a comparison of the multi-angle surface velocity distribution. Although the velocity of the search line tended to fluctuate near both sides of the bank where was a low velocity occurred, except for this, the difference from average velocity was almost within 10%. The standard deviation indicating the variation of the flow velocity was within 0.1 except for side bank. The cause of the difference in flow velocity near both banks was the lack of spatial resolution in the left bank and masking by plants in the right bank. According to Fujita et al. (2014), in STIV image analysis, it was difficult to analyze less than 0.4m/Pixel of the spatial resolution. Every image resolution of the UAV is 1920×1080 Pixel, however, for the slanted image, at the edge of the left bank, it was difficult to analyze because the spatial resolution was less than 0.3m/Pixel.

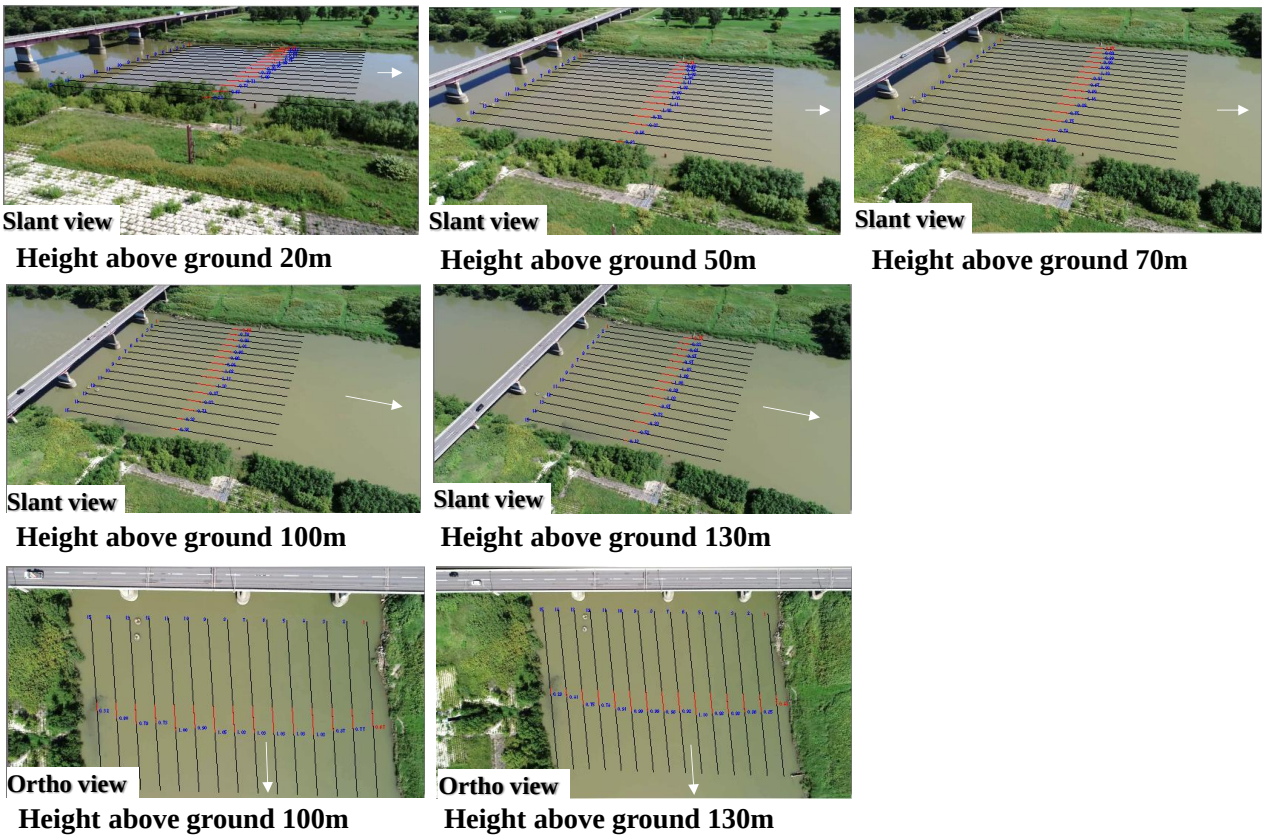

Figure 4. Comparison of flow velocity in multi-angle shots of UAV images

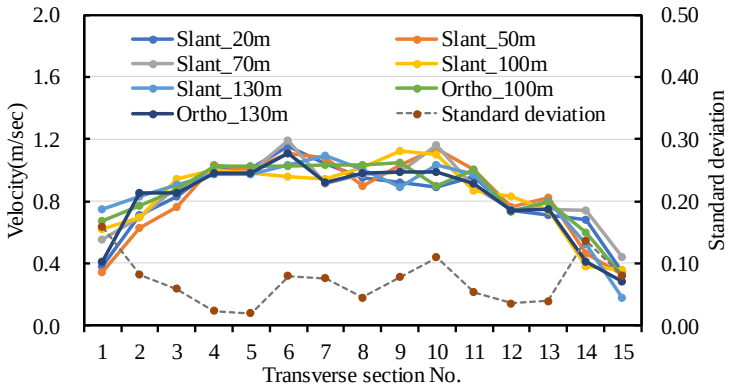

Figure 5. Velocity distribution and standard deviation of searching lines using surveying-GCP

3.4 Comparison of discharge in multi-angle image

The two methods were compared to discharge calculations. Type one is the divided sectional method of Japanese standard float measurement. Type two is a combination of measured velocity and numerical calculations. Type one is as follows in Figure 6(a); 1) Calculating the average flow velocity in the vertical direction of the surface velocity for each searching line × 0.85. 2) Dividing the transverse area so that the searching line is centered. 3) Multiply the divided transverse area by each flow velocity. 4) Summing up all the divided discharges. Type two is the Dynamic Interpolation and Extrapolation (DIEX) method by Nihei & Kimizu (2006) in Figure 6(b). This method is used for data assimilation observed surface velocities are interpolated or extrapolated into a river flow computation. The simplified fundamental equation for fluid motion is then expressed as Eq.(2).

$$gI + \frac{\partial}{\partial y}\left(A_H \frac{\partial u}{\partial y}\right) + \frac{1}{D^2}\frac{\partial}{\partial \sigma}\left(A_v \frac{\partial u}{\partial \sigma}\right) + F_a = 0 \tag{2}$$

Where y is the transverse direction, σ is the vertical direction, u is velocity in the streamwise (x) direction, D is water depth, g is the gravitational acceleration, I is the slope of the water elevation, and A_H and A_v are the horizontal and vertical eddy viscosities, respectively. Instead of the neglected terms such as advection terms in the equation, an additional term F_a is introduced, which compensates for the effects of the neglected terms. The added F_a is determined from the measured surface velocities to assimilate the field data into the numerical simulation. We set the discharge obtained from the equation (Eq.(3)) of the rating curve as a reference to compare the aerial STIV. For this gauging station, the rating curve was published every year to obtain between the observed discharge using type one method and the observed water stage. Then, we decided to use it of 2018's. The uncertainty of discharge between 2018's rating curve and the observed was within ±4%.

$$Q = 116.02 \times (H - 17.91)^2 \tag{3}$$

Where, Q; discharge(m^3/s), H; water level(m)=19.23m

According to Eq.(3), the reference discharge by the rating curve was 202.15 m^3/s. All discharges of type one (Divided sectional method) were within ±5% against the reference flow (202.15 m^3/s) in Figure 7(a) regardless of the multi-angle shot by UAV. All discharges of Type two (DIEX method) were slightly smaller than the rating curve and uncertainty of discharge was within -5%. As a result, the uncertainty of image discharge (within ± 5%) regardless of type one and type two was similar to uncertainty of discharge of the rating curve (within ±4%).

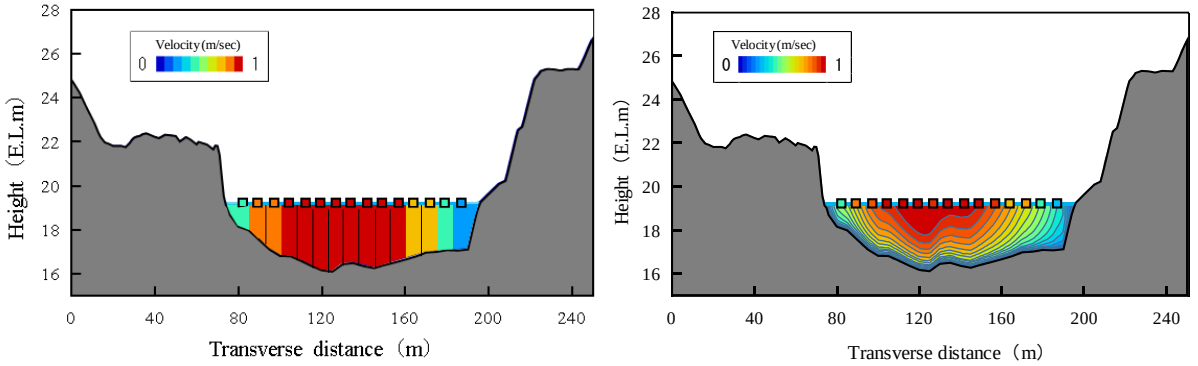

(a) Type one (Divided sectional method) (b) Type two (DIEX method)

Figure 6. Concept for discharge calculation method

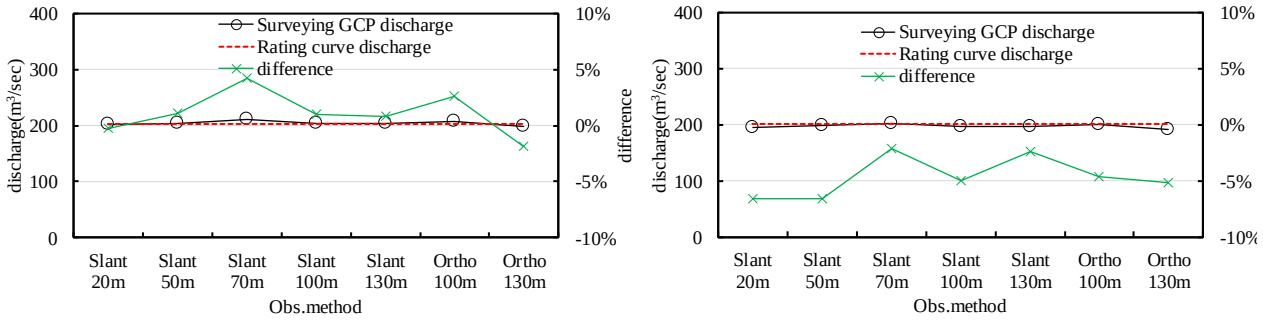

(a) Type one (Divided sectional method) (b) Type two (DIEX method)

Figure 7. Discharge in multi-angle using surveying-GCP

4. THE METHOD OF NONE GCP BY AERIAL STIV

4.1 Pseudo-GCP using SfM/MVS

Firstly, we conducted by UAV a zigzag flight about every 30m in the 300m longitudinal distance and 250m transverse distance as shown in Figure 8. Side lap was set to 70% and overlap was set to 85%. The total flight distance was 3700m and the flight time was 21 minutes. All sessions were completed on one flight, and the batteries were not replaced. Secondly, the 3D terrain model was created using SfM/MVS, and we extracted the pseudo-GCP from the point cloud instead of surveying-GCP as shown in Figure 9. In order to compare the accuracy of surveying-GCP and pseudo-GCP, we extracted 7 points at the same position. Pseudo-GCP was extracted as a point cloud in the 3D terrain model. Then, this GCP was plotted in Figure 9. As Figure 10, the difference of representative 2point distance between pseudo-GCP and surveying-GCP showed in 3 cases. The plane position error at the distance of 88m, 47m, and 143m was from 0.05m to 0.09 m. The height error was from 0.01m to 0.04m.

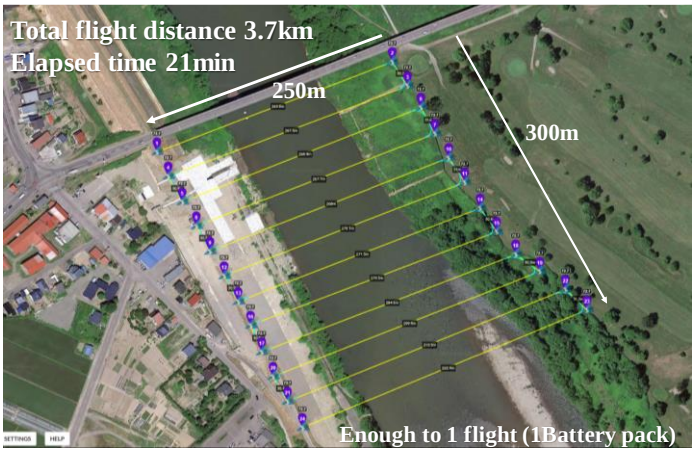

Figure 8. UAV flight tracking to make a 3D terrain model

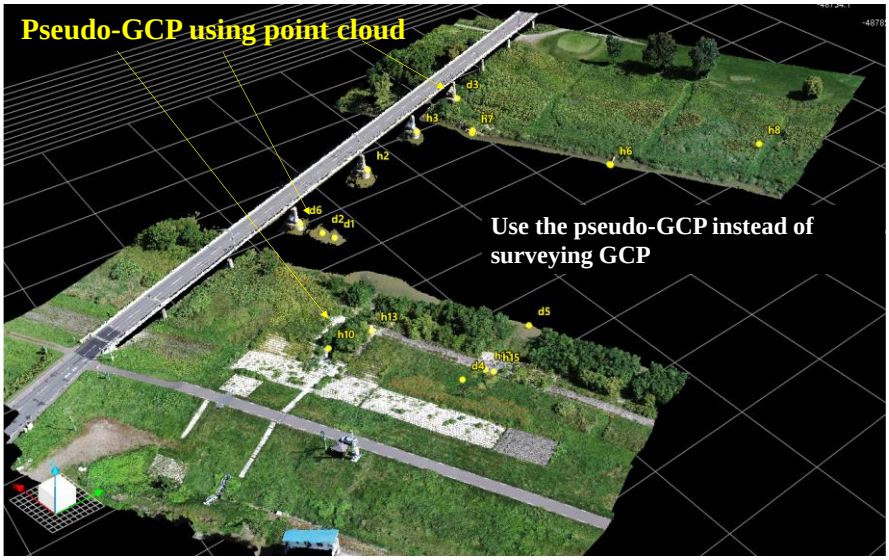

Figure 9. 3D terrain model by SfM/MVS

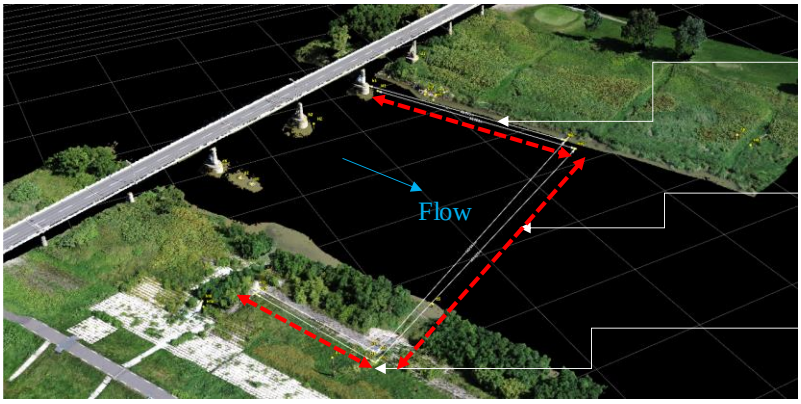

Unit:(m)

distance	Pseudo-GCP	TS surveying	difference
Horizontal	88.03	87.94	0.09
longitudinal	88.10	88.01	0.09
Height	3.38	3.39	-0.01

distance	Pseudo-GCP	TS surveying	difference
Horizontal	142.86	142.93	-0.07
longitudinal	142.95	143.02	-0.07
Height	5.27	5.28	-0.01

distance	Pseudo-GCP	TS surveying	difference
Horizontal	47.14	47.20	-0.05
longitudinal	47.14	47.20	-0.05
Height	0.04	-0.08	-0.04

Figure 10. Difference of the distance between pseudo-GCP and surveying- GCP

4.2 Comparison of discharge between pseudo-GCP and surveying-GCP

The velocity distribution used pseudo-GCP at the multi-angle was similar to the surveying-GCP as showed in Figure 11. The velocity of the search line exceeded the standard deviation of 0.1 on the right bank (No. 15) where the flow velocity was 0.3 m/s or less. However, the standard deviation of the other searching lines was within 0.1. We compared the average velocity of the multi-angle view used pseudo-GCP with average velocity used surveying-GCP in Figure 12. Except for the flow velocity within 0.4m/s, the different rate of other flow velocity was within approximately 10%. Comparing the discharge result of the pseudo-GCP with the surveying-GCP, The difference was less than 5% as shown in Figure12. Discharges of type one using pseudo-GCP were within ± 5% against the reference flow (202.15 m3/s) in Figure 13(a). On the other hand, discharges of type two using pseudo-GCP were within ± 5%, except for a low altitude (20m, 50m) in Figure 13(b). As a result, the comparison between the discharges of pseudo-GCP and surveying-GCP was shown that the difference was within 5% regardless of the divided sectional method or DIEX method.

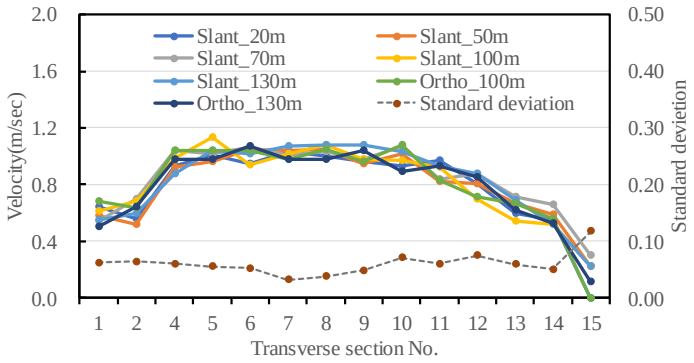

Figure 11. Velocity distribution and standard deviation of searching lines using pseudo-GCP

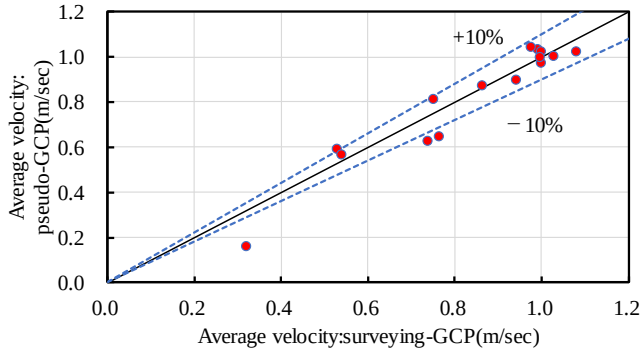

Figure 12. Average velocity of searching lines between pseudo-GCP and surveying-GCP

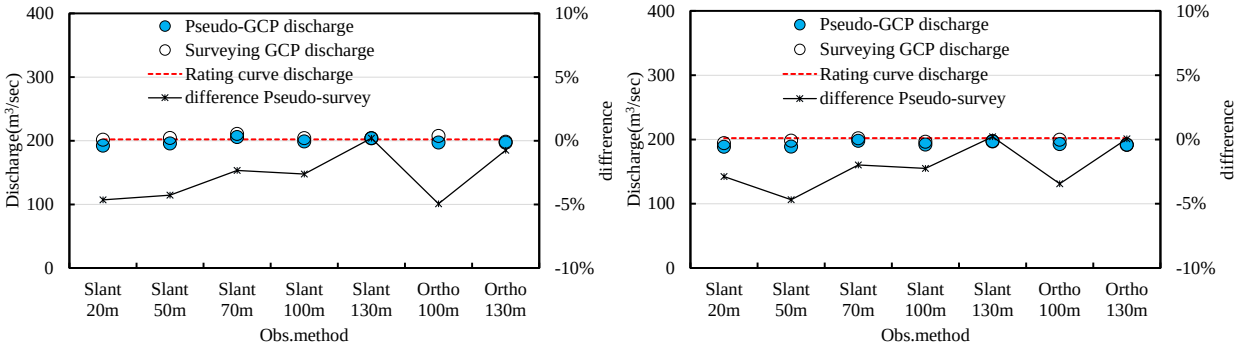

(a) Type one (Divided sectional method) (b) Type two (DIEX method)

Figure 13. Discharge in multi-angle using pseudo-GCP

5. CONCLUSIONS

- Whether UAV altitude (20-130m) or slant or orthoimage, the flow velocity calculated by the STIV method was matched less than 0.1 of standard deviation except for less than 0.4m /s.
- Besides, the discharge was less than 5% in every multi-angle view when compared with the discharge by the stage-discharge rating curve.
- UAV flight of 70% side laps and 85% overlap was able to create a 3D terrain model.
- UAV was possible to about 20 minutes flight to create a terrain model of 300m x 250m.
- In this terrain model, the plane position error at the distance was from 0.05m to 0.09 m and the height error was from 0.01m to 0.04m.
- The difference in surface flow velocity was within approximately 10%. Comparing the discharge result of the pseudo-GCP with the surveying-GCP, the difference was less than 5%, regardless of the divided sectional method and DIEX method
- A comparison of the discharge between using the pseudo GCP and surveying-GCP was shown that the difference was within ± 5%, regardless of the divided sectional method or DIEX method.

ACKNOWLEDGMENTS

We would like to express our deepest gratitude to Sapporo Development and Construction Department, Hokkaido Reginal Development Bureau.

REFERENCES

Andrew M. Cunliffea, Richard E. Braziera, Karen Anderson(2016) Ultra-fine grain landscape-scale quantification of dryland vegetation structure with drone-acquired structure-from-motion photogrammetry, *Remote Sensing of Environment*,183 (2016) 129–143.

Bemis,S.P.,Micklethwaite,S..Turner,D.et al.(2014) Ground-Based photogrammetry: a multi-scale, high-resolution mapping tool for structural geology and paleoseismology, Journal of Structural Geology,69,pp.163-pp.178.

Fujita I., Watanabe H. and Tsubaki R. (2007). Development of a non-intrusive and efficient flow monitoring technique: The space-time image Velocimetry (STIV), *International Journal of River Basin Management*:5(2), pp.105-114.

Fujita I., Kitada M.,Shimono M.,Kitsuda T.,Yorozuya A. and Motonaga Y. (2014). Spatial measurement of snow melt flood by image analysis with multiple-angle images and radio-controlled ADCP, *Journal of Japan Society of Civil Engineers, Ser. B1(Hydraulic Engineering),Vol.70,No.4:* Ⅰ_613-Ⅰ_618.

Fujita I., Notoya Y. and Shimano M. (2015). Development of UAV-based river surface velocity measurement by STIV based on high-accurate image stabilization techniques, *E-proceedings of the 36th IAHR World Congress*: 808014.pdf.

Fujita I., Notoya Y. and Tateguchi S. (2016). Development of efficient image stabilization algorithm for airborne video images and its application to river flow measurements, *River Flow 2016*, pp.548-554.

Fujita I, Deguchi T, Doi K, Ogino D, Notoya Y, Tateguchi S (2017). Development of KU-STIV: software to measure surface velocity distribution and discharge from river surface images. In: Proceedings of the 37th IAHR world congress, pp 5284–5292.

Koci J,Jarihani B, Leon JX, Slidle RC, Wilinson SN, Bartley R.(2017) Assessment of UAV and Ground-Based Structure from Motion with Multi-View Stereo Photogrammetry in a Gullied Savanna Catchment, ISPRS International Journal of Geo-Information 6: 328. DOI: https://doi.org/10.3390/ijgi6110328.

Natan Micheletti, Jim H Chandler, Stuart N Lane(2015) Structure from Motion (SfM) Photogrammetry, British Society for Geomorphology: Geomorphological Techniques, Chap. 2, Sec. 2.2.

Nihei, Y. and Kimizu, A. (2006), Evaluation of river velocity and discharge with a new assimilated method, Journal of River Basin Management, 4(1), 1-4.

Ryan,J.C.,Hubbard,A.L.,Box,J.E.et al.(2015) UAV photogrammetry and structure from motion to assess calving dynamics at Store Glacier, a large outlet draining the Greenland ice sheet, *The Cryosphere*,9(1),14-11.